Since January 2020 Elsevier has created a COVID-19 resource centre with free information in English and Mandarin on the novel coronavirus COVID-19. The COVID-19 resource centre is hosted on Elsevier Connect, the company's public news and information website.

Structure
Article

Direct Observation of Distinct A/P Hybrid-State tRNAs in Translocating Ribosomes

John F. Flanagan IV,[1,4] Olivier Namy,[2,4] Ian Brierley,[3,*] and Robert J.C. Gilbert[1,*]
[1]Division of Structural Biology, Henry Wellcome Building for Genomic Medicine, University of Oxford, Roosevelt Drive, Oxford OX3 7BN, UK
[2]Institut de Genetique et Microbiologie, Université Paris-Sud, batiment 400, 91405 Orsay Cedex, France
[3]Division of Virology, Department of Pathology, University of Cambridge, Tennis Court Road, Cambridge CB2 1QP, UK
[4]These authors contributed equally to this work
*Correspondence: ib103@mole.bio.cam.ac.uk (I.B.), gilbert@strubi.ox.ac.uk (R.J.C.G.)
DOI 10.1016/j.str.2009.12.007

SUMMARY

Transfer RNAs (tRNAs) link the genetic code in the form of messenger RNA (mRNA) to protein sequence. Translocation of tRNAs through the ribosome from aminoacyl (A) site to peptidyl (P) site and from P site to exit site is catalyzed in eukaryotes by the translocase elongation factor 2 (EF-2) and in prokaryotes by its homolog EF-G. During tRNA movement one or more "hybrid" states (A/P) is occupied, but molecular details of them and of the translocation process are limited. Here we show by cryo-electron microscopy that a population of mammalian ribosomes stalled at an mRNA pseudoknot structure contains structurally distorted tRNAs in two different A/P hybrid states. In one (A/P′), the tRNA is in contact with the translocase EF-2, which induces it. In the other (A/P″), the translocase is absent. The existence of these alternative A/P intermediate states has relevance to our understanding of the mechanics and kinetics of translocation.

INTRODUCTION

Protein synthesis at the ribosome involves the translation of a messenger RNA (mRNA), which is threaded through the space between the small and large ribosomal subunits (in eukaryotes, 40S and 60S). The amino acids are delivered to the ribosome by adaptor molecules called transfer RNAs (tRNAs), which recognize triplet codons of nucleic acid bases on mRNA with their anticodons. The tRNAs occupy a series of specific positions in the intersubunit space, known as the aminoacyl (A), peptidyl (P), and exit (E) sites. Translocation of tRNAs between these sites while still attached to the mRNA is the basis of ribosomal processivity along the mRNA and the maintenance of a single reading frame (Moazed and Noller, 1989; Rodnina et al., 1997). After peptide bond formation, the acceptor ends of the A and P site tRNAs move with respect to the large ribosomal subunit, but the anticodon ends remain in their original positions relative to the small ribosomal subunit, to yield hybrid-state tRNA intermediates P/E and A/P (Moazed and Noller, 1989). This process is facilitated by ratcheting of the ribosome, whereby the small and large subunits rotate with respect to one another by ~6° (Frank and Agrawal, 2000). Complete translocation of the mRNA-tRNA complex into the E and P sites is catalyzed by a monomeric G protein, elongation factor 2 (EF-2), with associated GTP hydrolysis (Noller et al., 2002; Wilden et al., 2006). The finite occupation by translocating tRNAs of an A/P hybrid state has been demonstrated by kinetic methods (Dorner et al., 2006) and represents one of a series of hybrid positions that have been inferred between both A and P and P and E sites. Although kinetic and biophysical studies have been especially important in identifying hybrid states (Rodnina et al., 1997; Wilden et al., 2006; Dorner et al., 2006; Blanchard et al., 2004; Pan et al., 2007), cryo-electron microscopy (cryo-EM) has also allowed their visualization, including a P/E hybrid state with the tRNA anticodon in the P site and acceptor arm in the E site (Taylor et al., 2007) and an A/P hybrid state close to the A site with a near-native tRNA conformation (Julián et al., 2008). Single-molecule kinetic studies have revealed that a number of kinetically distinct states are occupied by tRNAs during their passage from A to P sites (Wen et al., 2008). Indeed, we recently observed by cryo-EM a previously unanticipated A/P hybrid state tRNA with significant anticodon stem loop distortion (Namy et al., 2006). Our analysis was of an actively translating rabbit reticulocyte 80S ribosomal complex stalled by an mRNA pseudoknot structure (Brierley et al., 2007) derived from the programmed −1 ribosomal frameshifting signal of the coronavirus infectious bronchitis virus (IBV) (Brierley et al., 1989). In this complex, the hybrid state tRNA, which we termed A/P', is associated with EF-2 (Namy et al., 2006). The A/P' tRNA adopts a bent conformation as if it had the properties of a spring, and in this complex it was observed for the first time in direct contact with the translocase (Namy et al., 2006). On the basis of these observations we suggested that EF-2 acts as a Brownian ratchet within a "spring and ratchet" system to generate stepwise directional movement of the whole complex, facilitating translocation (Moran et al., 2008). The bending of the A/P' hybrid state observed by us (Namy et al., 2006) is similar to, but greater in magnitude than, that previously observed during tRNA accommodation into the A site (Valle et al., 2002). EF-2 seems to create this transition state prior to movement of tRNA into the P site proper (Namy et al., 2006; Moran et al., 2008) and the pause-step-pause movement of the ribosome-tRNA complex along the mRNA that this model infers is in agreement with the kinetics of single translocating ribosomes (Wen et al., 2008). The hybrid state

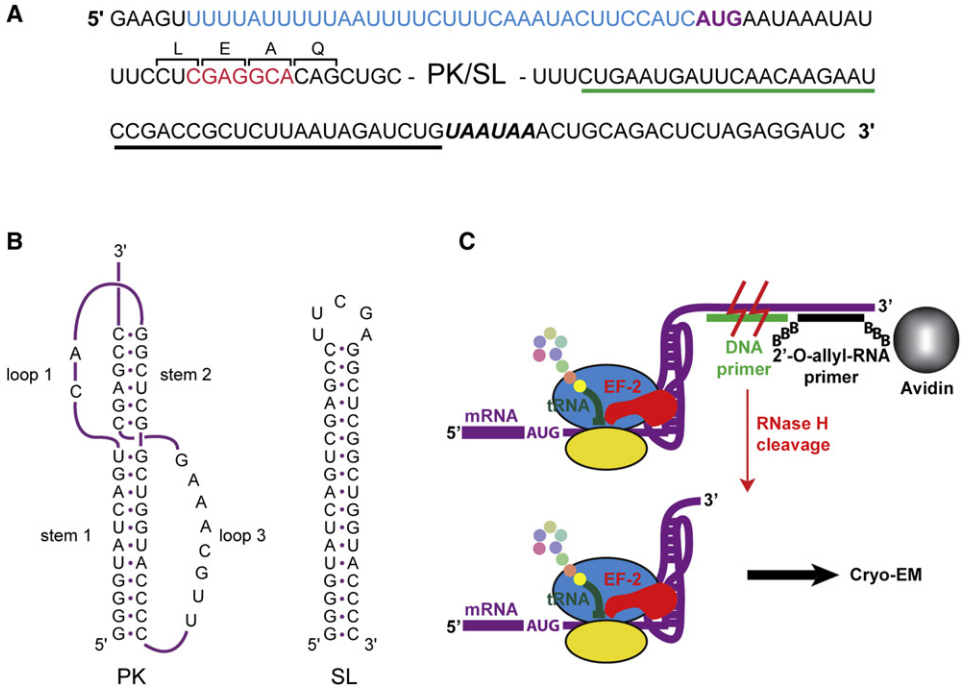

Figure 1. Sample Design and Purification

(A) mRNAs for in vitro translation contained the alfalfa mosaic virus RNA 4 unstructured leader (Jobling and Gehrke, 1987) (bases in blue), a start codon (AUG; purple), a pseudoknot (PK) or stem loop (SL), and a downstream region containing sequences complementary to DNA (underlined in green) or 2′-O-allyl RNA (underlined in black) oligonucleotides. Tandem translation termination codons were present near the end of the mRNA (UAA; bold and italicized). Bases in red occupy the position of the natural IBV slippery sequence, and the encoded amino acids in this region are indicated above the primary sequence.

(B) The sequences of the minimal IBV pseudoknot (PK) and related stem loop (SL) present in the mRNAs are shown.

(C) Following in vitro translation and pelleting through sucrose, stalled ribosomes were purified on an avidin matrix using a pre-annealed biotinylated 2′-O-allyl RNA oligonucleotide (black). Complexes were released by RNase H-directed cleavage using a complementary DNA primer (green) and subjected to cryo-EM.

giving rise to this interpretation is one that occurs in the presence of the translocase; the other A/P state since observed is an example of one that can form spontaneously (Julián et al., 2008).

In this paper we describe new structures of rabbit reticulocyte ribosomes stalled at the IBV pseudoknot (Brierley et al., 2007) and at a related stem loop that displays much reduced frameshifting efficiency. The stem loop-stalled ribosomes ($80S_{SL}$) contain a single tRNA in a canonical P site, as previously observed (Namy et al., 2006), while the pseudoknot-stalled ribosomes ($80S_{PK}$) contain structurally distorted tRNAs in two different A/P hybrid states. In the first (A/P′), the tRNA is in contact with the translocase EF-2, as previously observed (Namy et al., 2006), and appears to be in the process of translocation (Moran et al., 2008). In the second (A/P″), the tRNA is found in the absence of EF-2, but has failed to complete translocation and instead has, presumably, slipped back toward the A site. The existence of A/P′ and A/P″ hybrid states provides more direct, detailed information on tRNA trajectories than previously observed and we hypothesize that the translocase EF-2 may be able to cycle on to and off from the ribosome during a single round of translocation in a manner important for resolving secondary structures such as stem loops and pseudoknots within mRNAs.

RESULTS AND DISCUSSION

Overview of Reconstructed Complexes

Ribosome-mRNA complexes were assembled and purified as described in Figure 1 and in the Experimental Procedures. In vitro transcribed RNAs containing the IBV minimal pseudoknot or a related stem loop structure were translated in rabbit reticulocyte lysate (RRL) under conditions where the majority of ribosomes become stalled at these structures (Namy et al., 2006; see Supplemental Information available online). At this point, the complexes were stabilized by addition of cycloheximide, purified by affinity chromatography, and subjected to cryo-EM. A total of 38,720 images of the stem loop-stalled RRL ribosome ($80S_{SL}$) sample were analyzed and, selecting by tRNA occupancy (see Experimental Procedures), 24,738 (64%) of them were reconstructed to yield a reconstruction at 13.6 Å resolution (see below). This process of focused classification (Allen et al., 2005; Gilbert et al., 2007) made use of a spherical mask minimizing the chance of mask-induced bias in the image selection (see Supplemental Information). The data set of pseudoknot-stalled RRL ribosomes ($80S_{PK}$) consisted of 64,413 images and was initially reconstructed allowing for two ribosomal states: inactive and unbound by ligands or bound with an A/P′ hybrid state tRNA and EF-2 and engaged with the pseudoknot

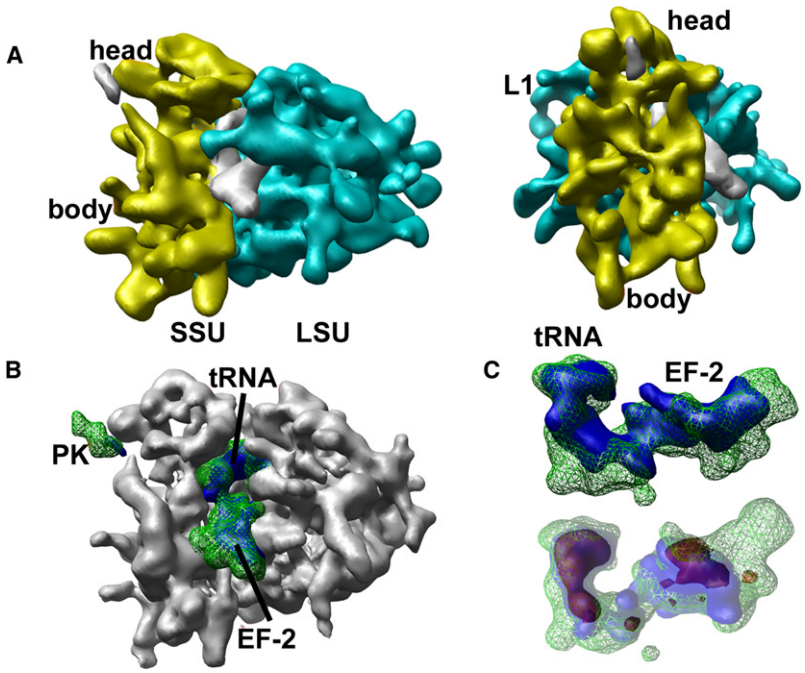

Figure 2. Initial Reconstruction and Assessment of Heterogeneity

(A) Orthogonal views of the initial $80S_{PK}$ structure determined using the data set described in this paper. Labeled are the large subunit (LSU; cyan) containing the L1 stalk and small subunit (SSU; yellow) containing the head and body. The difference density between the $80S_{PK}$ structure and an $80S_{Apo}$ ribosome is shown in white.

(B) The previously determined $80S_{Apo}$ reconstruction (Namy et al., 2006; gray surface) is shown superimposed with two difference maps. In green is the difference map for the previously determined $80S_{PK}$ complex versus the displayed empty form of the ribosome. The difference density illustrates the presence of the pseudoknot (PK), tRNA in a bent conformation (tRNA), and translocase (EF-2). In blue is the difference map obtained by aligning the new data set of $80S_{PK}$ images described in this paper with the displayed $80S_{Apo}$ map.

(C) Omit analysis of the tRNA and EF-2 density. The top panel shows the difference density for the tRNA and EF-2 portions of the structure, as in (B) (but rotated 90° counterclockwise), with the previously published difference map (Namy et al., 2006) colored green and that calculated from the new $80S_{PK}$ data set analyzed here in blue. The result of the omit analysis is shown in the bottom panel. The difference map for tRNA and EF-2 from the omit analysis is shown at two contour levels (blue and red) to demonstrate the relatively weak translocase density when the tRNA maintains its essential form. The green density is as above. The density for EF-2 is weaker and less well formed than that of the tRNA, indicating in the context of this omit analysis that they have different occupancies.

($80S_{PK\text{-}tRNA\text{-}EF\text{-}2}$) (Namy et al., 2006; Moran et al., 2008). The resulting maps were of limited resolution (~17 Å) for the data quality, given the resolution achieved with the $80S_{SL}$ complex from 24,738 images (13.6 Å) and had a weaker representation of EF-2 than for the tRNA (Figures 2A and 2B). This led us to hypothesize that the tRNA may have a higher occupancy in the sample than EF-2, as later demonstrated by omit analysis (Supplemental Information; Figure 2C). We therefore set about refining the $80S_{PK}$ data set into three groups (see Experimental Procedures), allowing for the ribosomes being either inactive ($80S_{Apo}$), stalled with a tRNA engaged with EF-2 ($80S_{PK\text{-}tRNA\text{-}EF\text{-}2}$), or stalled with a tRNA alone ($80S_{PK\text{-}tRNA}$). The refined $80S_{PK\text{-}tRNA\text{-}EF\text{-}2}$ reconstruction was calculated from 20,215/64,413 images (31%) to a resolution of 15.3 Å and the refined $80S_{PK\text{-}tRNA}$ reconstruction from 24,494/64,413 images (38%) to a resolution of 14.9 Å. Thus the PK-stalled complexes in the $80S_{PK}$ preparation account for 69% of the sample, as previously estimated in a two-way segmentation (Namy et al., 2006), which supports the validity of both our current image classification and the previously published results. The details of the $80S_{SL}$, $80S_{PK\text{-}tRNA\text{-}EF\text{-}2}$, and $80S_{PK\text{-}tRNA}$ complexes are discussed below. All resolutions in this paper have been estimated using the FSC = 0.5 criterion (Figure S1A). Some factors to consider in presenting cryo-EM reconstructions are the method by which the structure factor amplitudes are corrected and the contour level for map display. We corrected our data amplitudes along lines proposed by Rosenthal and Henderson (2003) (see Supplemental Information and Figure S1C). Our resolution estimate is confirmed by the presence of distinguishable RNA helices in our maps (Figure S1B). The conclusions of our work rely on assessment of the presence of EF-2 in our structures and the conformations of the tRNAs between the A and P sites of the intersubunit space. The omit analysis detailed above objectively addresses the question of the presence of EF-2 and tRNA, and our subsequent use of a supervised classification procedure shows there are two different kinds of hybrid state tRNA. We set the contour levels of all our maps by reference to the atomic model for a mammalian ribosome built on the basis of a canine ribosome reconstruction at 8.7 Å resolution (Chandramouli et al., 2008). This allowed us to encompass most of an atomic model based on this higher resolution structure within our maps. A few features remained outside the contoured surface, which were all at the periphery of the structure. We removed them from our atomic models when displaying them in the main paper but have shown them in Figure S2. We cannot be sure why these features are not clearly resolved in our maps but suspect this is due to either conformational flexibility or their being loosely associated with the ribosomes—both possibilities highlighted by their localization to the periphery of the structure (see Supplemental Information for more details).

Details of tRNAs Bound in the Complexes

Only a single tRNA is observed in the $80S_{PK}$ and $80S_{SL}$ complexes. Figure 3 shows the $80S_{SL}$, $80S_{PK\text{-}tRNA\text{-}EF\text{-}2}$, and $80S_{PK\text{-}tRNA}$ complexes in a standard view. In the $80S_{SL}$ reconstruction, the tRNA occupies the P site proper, into which it has successfully translocated. As in our previous analysis of this complex (Namy et al., 2006) we cannot see any density for the stem loop itself, which we think is due to its conformational flexibility. The affinity-based method of complex purification

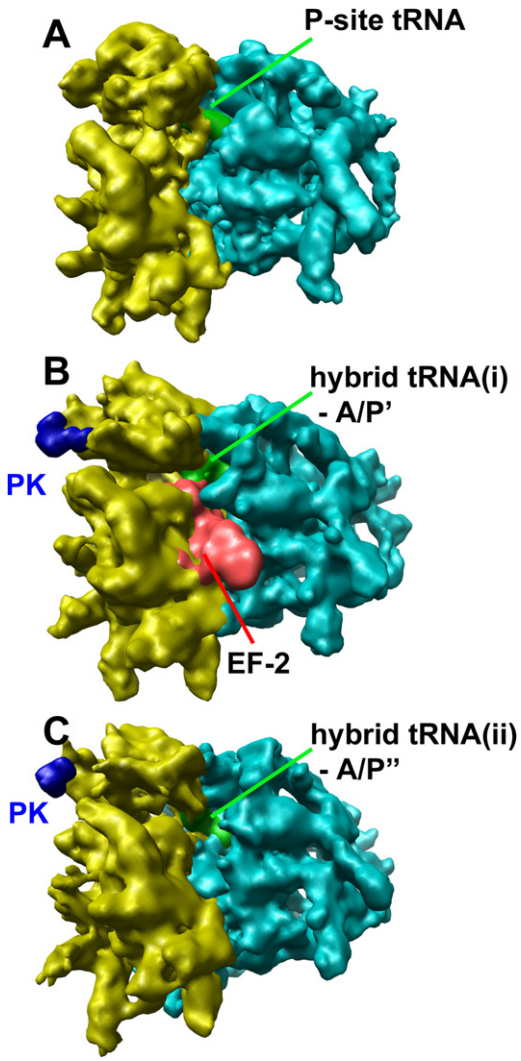

Figure 3. Refined Reconstructions of Pseudoknot and Stem Loop-Stalled Ribosomes

(A) Refined structure of the $80S_{SL}$ reconstruction. The small subunit is colored yellow and the large subunit blue, with the P site tRNA in green.

(B) As (A) for the $80S_{PK\text{-}tRNA\text{-}EF\text{-}2}$ complex, displaying the bent hybrid state tRNA in green, EF-2 in red, and the pseudoknot in blue.

(C) As (A) for the $80S_{PK\text{-}tRNA}$ complex, with the hybrid state tRNA again in green and the pseudoknot in blue.

(see Experimental Procedures) means that the stem loop-containing mRNA must be present in the ribosomal complexes. Further evidence that the ribosome particles used to compute this reconstruction are successfully stalled on the mRNA comes from the density present in the large subunit tunnel, which is consistent with an extended eight residue peptide (Figure 4A; Figures S3A–S3D) and matches that found in the PK-stalled complexes (Figure 4A). This suggests that all three complexes are successfully stalled and bound to the mRNA. Difference maps that compare programmed and empty ribosomes do not reveal any significant occupancy of the ribosomal A or E sites in our complexes. The lack of an A site tRNA probably reflects that these complexes are in, or approaching, a post-translocation state and, being stalled, have not refilled the A site. The absence of the E site tRNA may be explicable in terms of loss during the sucrose gradient and column chromatography steps of complex purification, as noted by others (Beckmann et al., 2001). Other possibilities include our use of cycloheximide to stabilize complexes or structural changes in the L1 stalk, either of which could influence E site occupancy (Pestova and Hellen, 2003; Márquez et al., 2004).

The PK-stalled maps contain tRNAs occupying broadly similar positions, between the A and P sites, and distorted in their anticodon arms (Figures 3B, 3C, and 4B; Figures S4A and S4B). The tRNA unengaged with EF-2 is bent significantly further, as if it has slipped or been pulled back toward the A site. We refer to the previously observed EF-2-engaged tRNA as being in an A/P′ state (Pan et al., 2007; Moran et al., 2008) and to the unengaged tRNA, by extension, as being in the A/P″ state. Averaging the density seen for EF-2 and the tRNA in the $80S_{PK\text{-}tRNA\text{-}EF\text{-}2}$ complex with that seen in the $80S_{PK\text{-}tRNA}$ complex gives density very similar to that seen in our previous analysis of this structure (Namy et al., 2006) (Figure S4C). This supports, as discussed above, that we have disentangled two different tRNA conformations and positions in the data set that were previously superimposed (Namy et al., 2006).

Insights from Fitting Atomic Structures to Reconstructed Densities

In order to interpret the conformations of the molecules bound within the stalled ribosomes in molecular detail, we made use of normal modes computable for atomic models (Tama et al., 2003, 2004) to fit the tRNAs and EF-2 to their respective densities (see Experimental Procedures). This allowed us to generate plausible models for A/P′ and A/P″ tRNAs and for the engaged EF-2 (Figures 4C and 4E), which firmly underscore the differences in tRNA conformation found between the various states observed in stem loop- and pseudoknot-stalled ribosomes. Engaged with EF-2, the A/P′ tRNA is compressed toward the intersubunit face of the 60S large subunit and the anticodon arm is bent, as seen previously (Namy et al., 2006) (Figure 4C, right panel). In the absence of EF-2, the tRNA is not pushed up toward the large subunit face or compressed, but has a dramatic bend toward the A site (clearly shown in Figure 4C, left panel; see also Figure S5A). Thus, tRNA compression toward the roof of the P site and bending of the anticodon arm in one direction is produced by EF-2, whereas anticodon bending in a different direction is likely created by pseudoknot-derived mRNA tension. Normal modes-assisted fitting of EF-2 showed domains I, II, and G' to have remained relatively rigid and to be similar in conformation to that found in Apo and sordarin-bound EF-2 (Jorgensen et al., 2003), but that domains III–V are rotated ~90° about them with respect to EF-2-sordarin (Figures 4D and 4E; Figures S5B–S5D). In the 80S ribosome bound with sordarin-fixed EF-2 (Spahn et al., 2004), the L1 stalk of the large subunit occludes the E site, but in our complex containing EF-2 in an active conformation we note that it remains open (Figure 5A). Thus tRNA procession out of the intersubunit space at the conclusion of translocation will be unhindered, providing another possible explanation for the lack of E site tRNAs in our stalled complexes as mentioned above. A distinctive feature of the EF-2-containing complex is the way in which the A site finger appears to be deployed over the join between EF-2 domains I, II, and G' and

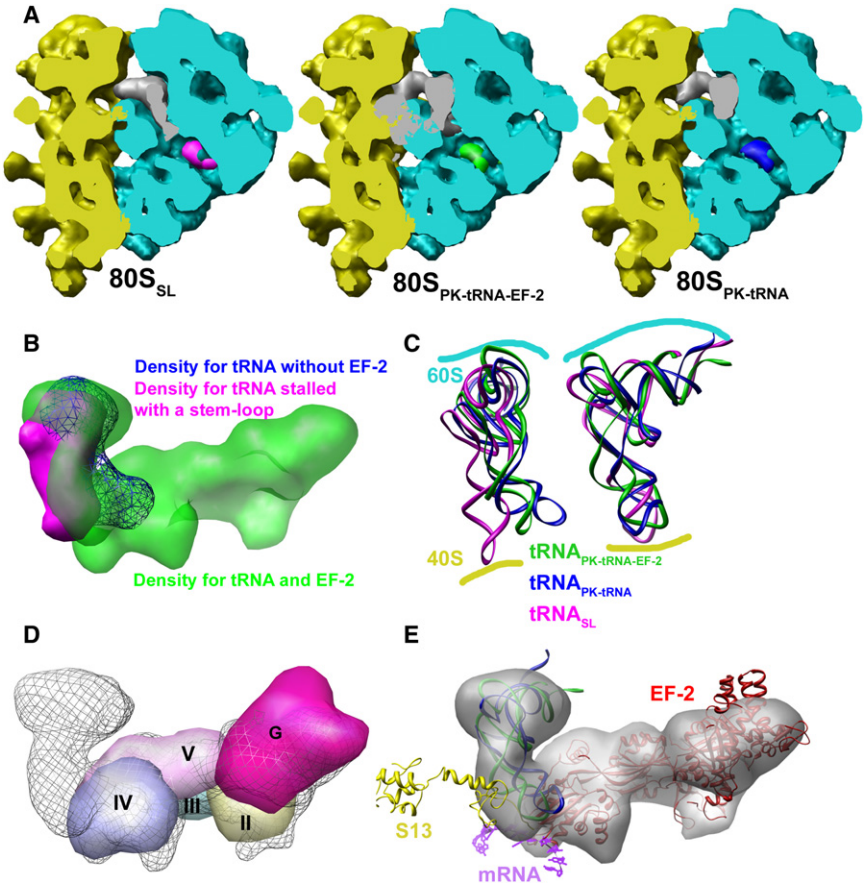

Figure 4. Nascent Protein, tRNA Conformations, and EF-2 As Observed in Pseudoknot-Stalled Complexes

(A) (Left) A view of the control reconstruction with the large subunit colored cyan and the small subunit colored yellow, with the tRNA density in the 80S$_{SL}$ complex (gray) and additional density arising from nascent protein (magenta). The control reconstruction is cut away with a rendered face to reveal the large subunit tunnel, bisected longitudinally. (Middle) As in left panel for the 80S$_{PK-tRNA-EF-2}$ map, showing the tRNA and EF-2 density in gray and the nascent protein in green. (Right) As left and middle panels for the 80S$_{PK-tRNA}$ map, showing tRNA in gray and the nascent protein in blue.

(B) Density arising from tRNA and EF-2 in the 80S$_{PK-tRNA-EF-2}$ complex (green), from tRNA in the 80S$_{PK-tRNA}$ complex (blue), and from tRNA in the 80S$_{SL}$ complex (magenta).

(C) tRNA atomic models fitted using normal modes to the 80S$_{PK-tRNA-EF-2}$ tRNA density (green), to the 80S$_{PK-tRNA}$ tRNA density (blue), and to the 80S$_{SL}$ tRNA density (magenta), in orthogonal views. The boundaries of the 40S and 60S subunits are indicated schematically.

(D) A comparison of the density deriving from tRNA and EF-2 bound in the 80S$_{PK-tRNA-EF-2}$ structure with a fit of EF-2 guided by normal modes (actual fit shown in E). The cryo-EM density is colored gray. The fitted crystal structure represented as a set of lobes of filtered density is as labeled.

(E) A composite view of the density for tRNA and EF-2 in the 80S$_{PK-tRNA-EF-2}$ structure (gray density), the fitted tRNAs with and without the presence of EF-2 (green and blue models, respectively, as in B), and the normal mode fitted EF-2 model (red). Also shown is the position of prokaryotic small subunit protein S13 (yellow; rpS18 in eukaryotes) and the mRNA (purple) with respect to the P site in this frame of reference, as resolved in the 70S X-ray structure (Selmer et al., 2006).

EF-2 domains III–IV (Figure 5B) in a manner consistent with its role as an attenuator of uncontrolled, out-of-register ribosomal movement (Korostelev et al., 2006; Komoda et al., 2006) since it appears thereby to fasten EF-2 within its binding site. EF-2 appears to remain in the stalled complex through the maintenance of native interactions with the elongating ribosome, which as a whole has been stalled by engagement with the pseudoknot. However, these interactions may be weaker than those holding the tRNAs in place, further within the intersubunit space, as suggested by the EF-2 partial occupancy.

As shown in Figure 4E, both the EF-2-engaged A/P′ tRNA and the A/P″ tRNA remain on the A site side of the gate between A and P sites formed by rpS18 (called S13 in prokaryotes) and a 45° mRNA kink (Selmer et al., 2006) as previously discussed (Moran et al., 2008). EF-2 seems to hold the A/P′ tRNA tight up against this gate and in this, to push the tRNA toward the intersubunit face of the 60S large subunit. The tautness of the 80S$_{PK-tRNA-EF-2}$ complex compared to the 80S$_{PK-tRNA}$ one is further indicated by the position of the pseudoknot, which juts out orthogonally from the proposed small subunit helicase center (Takyar et al., 2005; Namy et al., 2006) in the former case, but is relaxed downwards in the latter (Figures 3B and 3C). Thus, the movement of the A/P″ tRNA is consistent with a key role of the translocase to prevent slippage and to act by biasing forward translocation into the P site (Moran et al., 2008).

Biological Significance of Complexes

We have shown the translocase EF-2 is substoichiometric, bringing about the adoption of a novel A/P″ hybrid state, which joins the A/P′ state previously described (Namy et al., 2006) and the more recent A/P state occurring spontaneously (Julián et al., 2008) as A-to-P intermediates that have been seen directly. There are a number of possible explanations for the absence of EF-2 in ribosomal complexes containing the A/P″ hybrid state tRNA. These include that the hybrid state has arisen spontaneously before EF-2 has bound, that EF-2 was present but has been lost during complex purification, that tRNAs that have completed translocation can reverse translocate into this position, and that EF-2 can cycle off the ribosome during attempted translocation and then rejoin it to complete the process. While a spontaneously formed A/P″ tRNA is conceivable, it seems unlikely for several reasons: there is a high occupancy of it in the sample (38% in total, which corresponds to 55% of the stalled ribosomes), it has not previously been observed despite numerous studies of tRNA positions within the ribosome, and the tRNA is highly distorted. The possibility that EF-2 has fallen out of the complexes during their purification and thus induced the A/P″ state can be evaluated by reference to the completeness of the rest of the complexes. It is known that the accessory ribosomal protein RACK1 is peripherally associated with the small subunit head and that it is labile (Sengupta et al.,

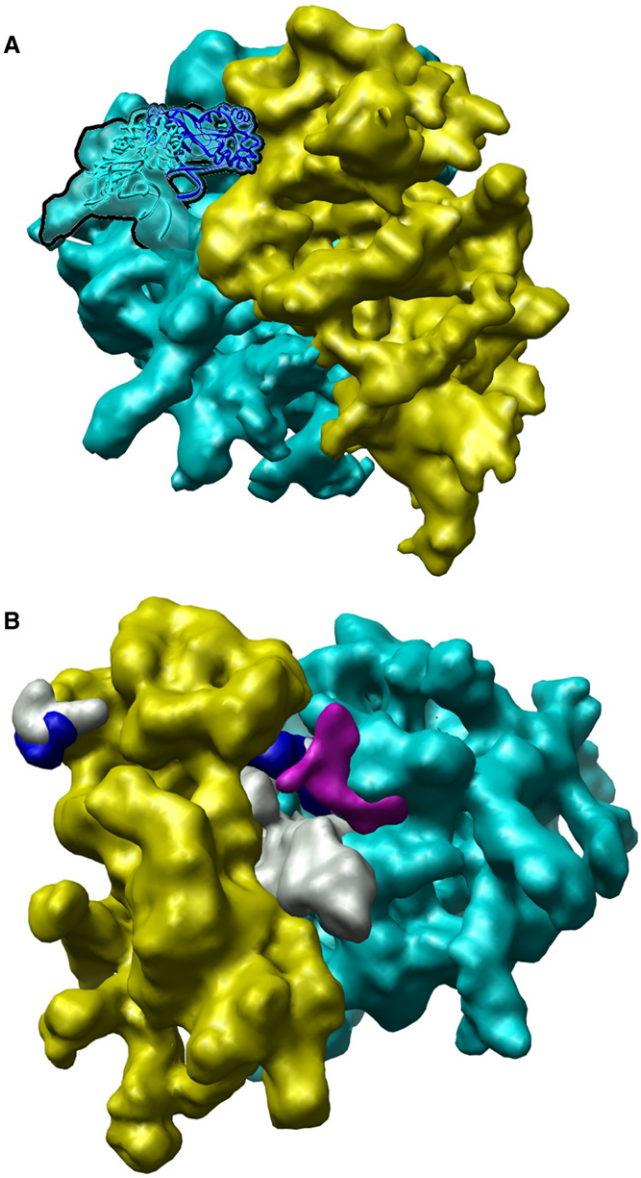

Figure 5. Conformational Differences in the Ribosome in Stalled Complexes

(A) A view of the $80S_{PK\text{-}tRNA}$ reconstruction with the subunits colored as before. The L1 stalk has been outlined in black and is fitted with atomic coordinates (cyan). The positioning of the stalk is quite different from that observed in the sordarin-stalled complex (atomic coordinates in blue) of Spahn et al. (2004).

(B) A composite view down the intersubunit space showing the ligands bound in the $80S_{PK\text{-}tRNA\text{-}EF\text{-}2}$ map in gray, those bound in the $80S_{PK\text{-}tRNA}$ map in blue, and difference density arising from the A-site finger in magenta. This density arises from the inserted A site finger.

2004), yet in all three stalled complexes, it is fully present, both in the reconstruction (Figure S3E) and as judged by western blotting (Figure S6). Since the rest of each ribosome appears by this test to be complete, it is likely that the EF-2 has not disassociated during purification. It seems unlikely that the A/P″ state could have arisen through spontaneous reverse translocation subsequent to successful placement of tRNA into the P site, because movement back over the A/P gate would have been uncatalyzed or otherwise unstimulated (Shoji et al., 2006; Konevega et al., 2007). We believe the most plausible hypothesis to be that the A/P″ state has arisen as a result of EF-2 enacting its reaction cycle without achieving completion of translocation. According to this explanation, EF-2 would bind and undergo GTP hydrolysis, induce a hybrid state such as A/P′, but leave before the P site has been reached, leading to backward slippage of the tRNA toward the A site and into the A/P″ state. Since the A/P″ tRNA-containing ribosomes identified in this study are not "dead-end" products—in translation assays virtually all IBV PK-stalled complexes chase to completion (Somogyi et al., 1993; Kontos et al., 2001)—this suggests that EF-2 can cycle repeatedly on to and off from the ribosome during single translocation steps. The likelihood of such cycling would be increased by the presence of mRNA secondary structures, especially mRNA pseudoknots, given their capacity to pause ribosomes (Somogyi et al., 1993) and their greater resistance to mechanical unfolding (Green et al., 2008).

Given that the pseudoknot used in this study derives from a viral ribosomal frameshifting signal, we have also considered whether the A/P″ state could arise following a frameshift event, which necessitates the physical separation of the tRNA anticodon from the mRNA. Consistent with this view, pseudoknot-induced mRNA tension is likely to put a strain on the codon-anticodon complex of the A/P′ hybrid state tRNA, and uncoupling of the tRNA from the mRNA would conceivably lead to loss of EF-2. However, the sequence of the mRNA in the decoding site of the stalled complexes studied here does not contain a slippery sequence (Jacks et al., 1988) and is GC rich (Namy et al., 2006; see Figure 1). Previous studies have shown that GC-rich stretches do not permit efficient RNA secondary structure-dependent frameshifting, and by analogy, the tRNAs decoding these sequences are less prone to detach from the mRNA (Jacks et al., 1988; Brierley et al., 1992). We thus consider the A/P″ state to have arisen as a result of the failure of EF-2 to complete translocation rather than as a consequence of an attempt to frameshift.

The observation of two different hybrid state tRNAs (A/P′ and A/P″) in our translocating complexes suggests that multiple, kinetically distinct steps govern translocation, centered on EF-2 binding, and detachment in two modes: prior to successful translocation and after it has occurred. In a single-ribosome kinetic study (Wen et al., 2008) it has recently been shown that ribosomes translocate through mRNA hairpins by stepwise movements separated by pauses. Measuring the times taken for translocation to occur and the dwell time (the time between translocation events, consisting of the pause time plus the translocation time), the authors were able to show that while the dwell time displays a distribution that indicates two or more successive rate-limiting processes, the translocation time appears to involve three similar or identical substeps (Wen et al., 2008). The different positions of translocating tRNAs that we observe would fit with these data.

Conclusion

By analyzing a pseudoknot-stalled population of ribosomes we show that they consist of three different states—an inactive, unoccupied state and two where tRNA is bound within the

complex. This is contrasted with a translocated tRNA seen in a stem loop-stalled ribosome, as well as a control reconstruction of an empty ribosome. In pseudoknot-stalled ribosomes, tRNAs are found in one of two different hybrid states between the A and P sites. These data suggest the existence of two discrete A/P hybrid tRNAs, one requiring the presence of EF-2 and the other its absence. Future experimental work will be needed to investigate the significance of our findings in greater detail.

EXPERIMENTAL PROCEDURES

Sample Preparation

Complexes were prepared and stored as previously described (Namy et al., 2006). Briefly, an mRNA (~200 nucleotides) containing the IBV minimal RNA pseudoknot or a related stem loop was preannealed to a biotinylated RNA oligonucleotide prior to in vitro translation in a RRL conducted at 27°C for 15 min. After the addition of cycloheximide to fix the complexes, ribosomes were pelleted through a sucrose cushion, resuspended, and applied to an avidin affinity column. Following extensive washing the stalled complexes were eluted by addition of RNase H and a DNA oligonucleotide complementary to a region of the mRNA immediately downstream of the pseudoknot (Figure 1). The complexes were flash frozen in liquid nitrogen and stored at −70°C. The sample generated by pseudoknot-mediated pausing is referred to below as $80S_{PK}$ and that generated by stem loop-mediated pausing as $80S_{SL}$.

Cryo-EM Data Collection

For imaging $80S_{PK}$ and $80S_{SL}$ complexes, 3 μl of each sample were aliquoted onto holey carbon grids (Agar Scientific; 0.015 A^{260} units per grid) following negative glow discharging. The grids were blotted and flash frozen in liquid ethane. Cryo-electron micrographs were taken at 39,000× magnification using an FEI F30 cryo-microscope, equipped with a Field Emission Gun and operating at 300 kV, in low dose mode with defocuses ranging from −0.8 to −3.6 μm. The micrographs were then scanned using a 7 μm raster on a Zeiss/Scai Photoscan scanner.

Data Analysis for the PK and SL-Stalled Ribosomes

Particles were boxed and the CTF corrected using EMAN suite programs (Ludtke et al., 1999). Reconstructions were performed with SPIDER (Frank et al., 1996), using projection matching-based alignment and focused classification (Allen et al., 2005; Gilbert et al., 2007) to separate the whole data sets into Apo versus stalled states and depending on the stoichiometry of the stalled complexes. A full description of the methods used is supplied in the Supplemental Experimental Procedures. Structure factor amplitude B factor correction was facilitated using WellMAP (J.F.F. and R.J.C.G., unpublished data).

Atomic Structure Fitting

Atomic models constructed for the dog 80S ribosome (Chandramouli et al., 2008) were used to fit the density arising from the two ribosomal subunits, splitting the models up to allow refinement of the fit of individual subunit domains (see Supplemental Information). Initial manual fits performed in O (Jones et al., 1991) were refined using URO (Navaza et al., 2002). Because the tRNAs and EF-2 had undergone significant conformational change, we made use of normal modes-assisted fitting in the program NMFF (Tama et al., 2003, 2004), the inferred elastic properties of the atomic models being used to morph them into corresponding density. See Supplemental Information for more details.

ACCESSION NUMBERS

Coordinates have been deposited in the European Bioinformatics Institute Macromolecular Structure Database with accession codes EMD-1670, EMD-1671, and EMD-1672.

SUPPLEMENTAL INFORMATION

Supplemental Information includes six figures and Supplemental Experimental Procedures and can be found with this article online at doi:10.1016/j.str.2009.12.007.

ACKNOWLEDGMENTS

This work was supported by grants from the Biotechnology and Biological Sciences Research Council UK and the Medical Research Council, UK. O.N. is supported by a grant from the Agence Nationale de la Recherche (ANR-06-BLAN-0391-01) and R.J.C.G. is a Royal Society University Research Fellow.

Received: May 30, 2009
Revised: October 28, 2009
Accepted: December 7, 2009
Published: February 9, 2010

REFERENCES

Allen, G.S., Zavialov, A., Gursky, R., Ehrenberg, M., and Frank, J. (2005). The cryo-EM structure of a translation initiation complex from *Escherichia coli*. Cell *121*, 703–712.

Beckmann, R., Spahn, C.M.T., Eswar, N., Helmers, J., Penczek, P.A., Sali, A., Frank, J., and Blöbel, G. (2001). Architecture of the protein-conducting channel associated with the translating 80S ribosome. Cell *107*, 361–372.

Blanchard, S.C., Kim, H.D., Gonzalez, R.L., Jr., Puglisi, J.D., and Chu, S. (2004). tRNA dynamics on the ribosome during translation. Proc. Natl. Acad. Sci. USA *101*, 12893–12898.

Brierley, I., Digard, P., and Inglis, S.C. (1989). Characterization of an efficient coronavirus ribosomal frameshifting signal: requirement for an RNA pseudoknot. Cell *57*, 537–547.

Brierley, I., Jenner, A.J., and Inglis, S.C. (1992). Mutational analysis of the "slippery-sequence" component of a coronavirus ribosomal frameshifting signal. J. Mol. Biol. *227*, 463–479.

Brierley, I., Pennell, S., and Gilbert, R.J.C. (2007). Viral RNA pseudoknots: versatile motifs in gene expression and replication. Nat. Rev. Microbiol. *5*, 598–610.

Chandramouli, P., Topf, M., Ménétret, J.P., Eswar, N., Cannone, J.J., Gutell, R.R., Sali, A.A., and Akey, C.W. (2008). Structure of the mammalian 80S ribosome at 8.7 Å resolution. Structure *16*, 535–548.

Dorner, S., Brunelle, J.L., Sharma, D., and Green, R. (2006). The hybrid state of tRNA binding is an authentic translation elongation intermediate. Nat. Struct. Mol. Biol. *13*, 234–241.

Frank, J., and Agrawal, R.L. (2000). A ratchet-like inter-subunit rearrangement of the ribosome during translocation. Nature *406*, 318–322.

Frank, J., Radermacher, M., Penczek, P., Zhu, J., Li, Y., Ladjadj, M., and Leith, A. (1996). SPIDER and WEB: processing and visualization of images in 3D electron microscopy and related fields. J. Struct. Biol. *116*, 190–199.

Gilbert, R.J.C., Gordiyenko, Y., von der Haar, T., Sonnen, A.F.-P., Hofmann, G., Nardelli, M., Stuart, D.I., and McCarthy, J.E.G. (2007). Reconfiguration of yeast 40S ribosomal subunit domains by the translation initiation multifactor complex. Proc. Natl. Acad. Sci. USA *104*, 5788–5793.

Green, L., Kim, C.H., Bustamante, C., and Tinoco, I., Jr. (2008). Characterization of the mechanical unfolding of RNA pseudoknots. J. Mol. Biol. *375*, 511–528.

Jacks, T., Madhani, H.D., Masiarz, F.R., and Varmus, H.E. (1988). Signals for ribosomal frameshifting in the Rous sarcoma virus *gag-pol* region. Cell *55*, 447–458.

Jobling, S.A., and Gehrke, L. (1987). Enhanced translation of chimaeric messenger RNAs containing a plant viral untranslated leader sequence. Nature *325*, 622–625.

Jones, T.A., Zou, J.Y., Cowan, S.W., and Kjeldgaard, M. (1991). Improved methods for binding protein models in electron density maps and the location of errors in these models. Acta Crystallogr. A *47*, 110–119.

Jorgensen, R., Ortiz, P.A., Carr-Schmid, A., Nissen, P., Kinzy, T.G., and Andersen, G.R. (2003). Two crystal structures demonstrate large conformational changes in the eukaryotic ribosomal translocase. Nat. Struct. Biol. *10*, 379–385.

Julián, P., Konovega, A.L., Scheres, S.H., Lázaro, M., Gil, D., Wintermeyer, W., Rodnina, M.V., and Valle, M. (2008). Structure of ratcheted ribosomes with tRNAs in hybrid states. Proc. Natl. Acad. Sci. USA *105*, 16924–16927.

Komoda, T., Sato, N.S., Phelps, S.S., Namba, N., Joseph, S., and Suzuki, T. (2006). The A-site finger in 23 S rRNA acts as a functional attenuator for translocation. J. Biol. Chem. *281*, 32303–32309.

Konevega, A.L., Fischer, N., Semenkov, Y.P., Stark, H., Wintermeyer, W., and Rodnina, M.V. (2007). Spontaneous reverse movement of mRNA-bound tRNA through the ribosome. Nat. Struct. Mol. Biol. *14*, 318–324.

Kontos, H., Napthine, S., and Brierley, I. (2001). Ribosomal pausing at a frameshifter RNA pseudoknot is sensitive to reading phase but shows little correlation with frameshift efficiency. Mol. Cell. Biol. *21*, 8657–8670.

Korostelev, A., Trakhanov, S., Laurberg, M., and Noller, H.F. (2006). Crystal structure of a 70S ribosome-tRNA complex reveals functional interactions and rearrangements. Cell *126*, 1065–1077.

Ludtke, S.J., Baldwin, P.R., and Chiu, W. (1999). EMAN: semiautomated software for high-resolution single-particle reconstructions. J. Struct. Biol. *128*, 82–97.

Márquez, V., Wilson, D.N., Tate, W.P., Triana-Alonso, F., and Nierhaus, K.H. (2004). Maintaining the ribosomal reading frame: the influence of the E site during translational regulation of release factor 2. Cell *118*, 45–55.

Moazed, D., and Noller, H.F. (1989). Intermediate states in the movement of transfer RNA in the ribosome. Nature *342*, 142–148.

Moran, S.J., Flanagan, J.F., IV, Namy, O., Stuart, D.I., Brierley, I., and Gilbert, R.J.C. (2008). The mechanics of translocation: a molecular ''spring-and-ratchet'' system. Structure *16*, 664–672.

Namy, O., Moran, S.J., Stuart, D.I., Gilbert, R.J.C., and Brierley, I. (2006). A mechanical explanation of RNA pseudoknot function in programmed ribosomal frameshifting. Nature *441*, 244–247.

Navaza, J., Lapault, J., Rey, F.A., Alvarez-Rúa, C., and Broge, J. (2002). On the fitting of model electron densities into EM reconstructions: a reciprocal space formulation. Acta Crystallogr. D Biol. Crystallogr. *58*, 1820–1825.

Noller, H.F., Yusupov, M.M., Yusupova, G.Z., Baucom, A., and Cate, J.H.D. (2002). Translocation of tRNA during protein synthesis. FEBS Lett. *514*, 11–16.

Pan, D., Kirillov, S.V., and Cooperman, B.S. (2007). Kinetically competent intermediates in the translocation step of protein synthesis. Mol. Cell *25*, 519–529.

Pestova, T.V., and Hellen, C.U.T. (2003). Translation elongation after assembly of ribosomes on the Cricket paralysis virus internal ribosome entry site without initiation factors or intiator tRNA. Genes Dev. *17*, 181–186.

Rodnina, M.V., Savelsbergh, A., Katunin, V.I., and Wintermeyer, W. (1997). Hydrolysis of GTP by elongation factor G drives tRNA movement on the ribosome. Nature *385*, 37–41.

Rosenthal, P.B., and Henderson, R. (2003). Optimal determination of particle orientation, absolute hand, and contrast loss in single-particle electron cryomicroscopy. J. Mol. Biol. *333*, 721–745.

Selmer, M., Dunham, C.M., Murphy, F.V., IV, Weixlbaumer, A., Petry, S., Kelley, A.C., Weir, J.R., and Ramakrishnan, V. (2006). Structure of the 70S ribosome complexed with mRNA and tRNA. Science *313*, 1935–1942.

Sengupta, J., Nilsson, J., Gursky, R., Spahn, C.M., Nissen, P., and Frank, J. (2004). Identification of the versatile scaffold protein RACK1 on the eukaryotic ribosome. Nat. Struct. Mol. Biol. *11*, 957–962.

Shoji, S., Walker, S.E., and Fredrick, K. (2006). Reverse translocation of tRNA in the ribosome. Mol. Cell *24*, 931–942.

Somogyi, P., Jenner, A.J., Brierley, I., and Inglis, S.C. (1993). Ribosomal pausing during translation of an RNA pseudoknot. Mol. Cell. Biol. *13*, 6931–6940.

Spahn, C.M.T., Gomez-Lorenzo, M.G., Grassucci, R.A., Jorgensen, R., Andersen, G.R., Beckmann, R., Penczek, P.A., Ballesta, J.P., and Frank, J. (2004). Domain movements of elongation factor eEF-2 and the eukaryotic 80S ribosome facilitate tRNA translocation. EMBO J. *23*, 1008–1019.

Takyar, S., Hickerson, R.P., and Noller, H.F. (2005). mRNA helicase activity of the ribosome. Cell *120*, 49–58.

Tama, F., Valle, M., Frank, J., and Brooks, C.L., III. (2003). Dynamic reorganization of the functionally active ribosome explored by normal mode analysis and cryo-electron microscopy. Proc. Natl. Acad. Sci. USA *100*, 9319–9323.

Tama, F., Miyashita, O., and Brooks, C.L., III. (2004). Normal mode based flexible fitting of high-resolution structure into low-resolution experimental data from cryo-EM. J. Struct. Biol. *147*, 315–326.

Taylor, D.J., Nilsson, J., Merrill, A.R., Andersen, G.R., Nissen, P., and Frank, J. (2007). Structures of modified eEF2 80S ribosome complexes reveal the role of GTP hydrolysis in translocation. EMBO J. *26*, 2421–2431.

Valle, M., Sengupta, J., Swami, N.K., Grassucci, R.A., Burkhardt, N., Nierhaus, K.H., Agrawal, R.K., and Frank, J. (2002). Cryo-EM reveals an active role for aminoacyl-tRNA in the accommodation process. EMBO J. *21*, 3557–3567.

Wen, J.D., Lancaster, L., Hodges, C., Zeri, A.C., Yoshimura, S.H., Noller, H.F., Bustamante, C., and Tinoco, I. (2008). Following translation by single ribosomes one codon at a time. Nature *452*, 598–603.

Wilden, B., Savelsbergh, A., Rodnina, M.V., and Wintermeyer, W. (2006). Role and timing of GTP binding and hydrolysis during EF-G-dependent tRNA translocation on the ribosome. Proc. Natl. Acad. Sci. USA *103*, 13670–13675.

